Gram-Scale Synthesis of Ultrathin Tungsten Oxide Nanowires and their Aspect Ratio-Dependent Photocatalytic Activity

Jincheng Liu, Olivier Margeat, Walid Dachraoui, Xianjie Liu, Mats Fahlman, and Jorg Ackermann**

Preparation of size-tunable ultrathin $W_{18}O_{49}$ nanowires by an alcohol-assisted solvothermal decomposition of tungstic acid is reported. The synthesis of ultrathin $W_{18}O_{49}$ nanowires can be achieved at large scale and low cost, while changing the molecular size of the used alcohols can control the nanowire morphology. With increasing the molecular size of the alcohol, the synthesized $W_{18}O_{49}$ nanowires have smaller diameters and longer lengths. The as-prepared blue $W_{18}O_{49}$ nanomaterials show a very strong visible light absorption caused by oxygen defects and an aspect ratio-dependent photocatalytic activity on the degradation of pollutant rhodamine B (RhB) under simulated solar light irradiation. It is found that the $W_{18}O_{49}$ nanowires with highest aspect ratio show the highest activity in the photodegradation of RhB, which could be related to their higher density of oxygen surface defects in combination with a higher adsorption capability of RhB. This new synthetic route of size tunable ultrathin $W_{18}O_{49}$ nanomaterials will enlarge their potential applications and can be possibly used in the pyrolyzing synthesis of other metal oxide nanomaterials.

1. Introduction

One dimensional (1-D) ultrathin nanowires with a diameter less than 3 nm are currently of great interest because of their high surface area, reduced grain boundaries, direct charge transfer pathways, and strong quantum size effects.[1,2] Through the methodologies of templating, ligand control, and oriented attachment, various kinds of ultrathin nanowires can be synthesized.[3] However, the gradual control of diameter and length of ultrathin nanowires as well as the corresponding synthesis approaches working on large scale are still a big challenge, which limits the extensive applications of ultrathin nanowires.

Monoclinic tungsten trioxide ($W_{18}O_{49}$) with a small bandgap between 2.4 and 2.8 eV is an important type of semiconductor, covering wide application domains such as electrochromic devices, gas sensors, or photocatalysts.[4–6] Focusing on the photocatalytic process, the activity is significantly affected by the diffusion length of photogenerated charge carriers, the surface area, and the aspect ratios of $W_{18}O_{49}$ nanomaterials.[7] Because ultrathin nanowires have a short charge diffusion length and a large surface generating more reactive surfaces, it can be expected that ultrathin $W_{18}O_{49}$ nanowires may have promising photocatalytic properties.

Up to date, one dimensional $W_{18}O_{49}$ ultrathin nanocrystals were synthesized by the alcoholysis of tungsten chlorides (WCl_6),[8,9] tungsten alkoxides,[10] or tungsten carbonyls [$W(CO)_6$] precursors by bottom-up approaches.[11] However, all those synthetic methods of $W_{18}O_{49}$ ultrathin nanowires are limited to small quantities by using expensive tungsten precursors and do not allow controlling aspect ratios, thus limiting their use in future applications in the field of nanotechnology.

In this work, we report a new gram-scale synthesis of ultrathin (1–3 nm) $W_{18}O_{49}$ nanowires by a solvothermal method using non-toxic tungstic acid precursors. Importantly, this new top-down approach based on the decomposition of laminated tungstic acid precursors allows controlling both length and diameter of the $W_{18}O_{49}$ nanowires by a simple change of alcohol used during synthesis. Indeed, intercalation of alcohols of different molecular size assists the laminated tungstic acid precursors to decompose into ultrathin $W_{18}O_{49}$ nanowires of controlled aspect ratios. Furthermore, a detailed study of this new top-down synthesis is presented to understand the underlying growth mechanism and to correlate it to the observed diameters and lengths.

Nontoxic sodium tungstate and tungstic acid are known and widely used in the synthesis of WO_3 nanorods[12–15] and WO_3 nanowires[16–18], but only with large diameters, and could not so far be applied to the synthesis of ultrathin one-dimensional

Dr. J. Liu, Dr. O. Margeat, Dr. W. Dachraoui, Dr. J. Ackermann
Aix-Marseille Université
CNRS, CINaM UMR 7325, 13288, Marseille, France
E-mail: olivier.margeat@univ-amu.fr; ackermann@cinam.univ-mrs.fr
Dr. J. Liu
Department of Polymer Science & Engineering
Huaqiao University
Xiamen 361021, China
Dr. X. Liu, Prof. M. Fahlman
Department of Physics, Chemistry and Biology
Linkoping University
58183, Linkoping, Sweden

DOI: 10.1002/adfm.201401261

$W_{18}O_{49}$ nanocrystals. We thus report for the first time that alcohol-intercalation can assist laminated tungstic acid precursors to decompose into ultrathin $W_{18}O_{49}$ nanorods and nanowires using a solvothermal method. To the best of our knowledge, it is the first time that ultrathin $W_{18}O_{49}$ nanowires can be synthesized from tungstic acid precursors by a top-town method. The as-prepared one-dimensional $W_{18}O_{49}$ nanocrystals are then used in a comparative photocatalytic degradation study of rhodamine B (RhB) under simulated solar light irradiation. The aspect ratio-dependence of the photocatalytic activity of these one-dimensional $W_{18}O_{49}$ nanocrystals is described for the first time and discussed.

2. Results and Discussion

2.1. Synthesis and Characterization of One-Dimensional $W_{18}O_{49}$ Nanocrystals

First, tungstic acid (H_2WO_4) precursors were prepared by a one step reaction from Na_2WO_4 aqueous solution and diluted HNO_3 solution. The prepared H_2WO_4 precursors were then used in the synthesis of $W_{18}O_{49}$ with different treatments prior to adding oleylamine and heating. Only aggregated WO_3 materials with big sizes were obtained in the synthesis from the totally dried H_2WO_4 precursors and wet H_2WO_4 precursors with residual water (Figure S1a,b, Supporting Information). After exchanging residual water by acetone, the prepared WO_3 synthesis resulted mainly in big nanorods with a diameter of 20–30 nm without purging argon (Figure S1c, Supporting Information), and large particles in addition to some nanorods and few thin nanowires with purging argon (Figure S1d, Supporting Information). The presence of thin nanowires at this stage inspired to further continue exchanging the water in the deposited H_2WO_4 by different kinds of alcohols. Interestingly, the resulting $W_{18}O_{49}$ nanocrystals obtained by different alcohols could be well dispersed in toluene and chloroform making their morphological study by transmission electron microscopy (TEM) highly accessible for a detailed analysis. **Figure 1** shows TEM images of prepared $W_{18}O_{49}$ nanocrystals by wet H_2WO_4 precursors with the exchange of water by methanol, ethanol, isopropanol, and benzyl alcohol. It is clearly shown that, with the exchange of water by all those alcohols, uniform one-dimensional $W_{18}O_{49}$ nanocrystals can be obtained. When using wet H_2WO_4 with methanol, $W_{18}O_{49}$ nanorods with a diameter of ≈2.3–3.3 nm and a length of around 50 nm are obtained (sample S-$W_{18}O_{49}$ NR). With the exchange of water by ethanol, $W_{18}O_{49}$ medium-sized nanowires are synthesized with a diameter of ≈2–2.3 nm and a length of 100 nm. When using isopropanol, we observe $W_{18}O_{49}$ nanowires with diameters of ≈1.7–2 nm and a length of ≈120–150 nm (sample M-$W_{18}O_{49}$ NW). The nanowires show clear lattice fringes and an interplanar *d*-spacing of 0.378 nm (Figure 1d), which is in good agreement with the (010) lattice fringes of the monoclinic phase of $W_{18}O_{49}$.[19,20] The synthesized $W_{18}O_{49}$ nanowires are thus single crystals with growth along the [010] direction.[21]

Importantly, the use of wet H_2WO_4 with benzyl alcohol leads to much longer $W_{18}O_{49}$ nanowires with a decrease of the diameter down to 1.4 nm and a length up to 400 nm as seen on Figure 1e. A very high aspect ratio of almost 300 is thus obtained (long nanowires sample named L-$W_{18}O_{49}$ NW). In conclusion, the TEM observation reveals that the exchange of water by alcohols with increased molecular size leads to $W_{18}O_{49}$ nanowires of increased aspect ratio. Thus, simple changes of the alcohols during synthesis allow controlling the diameter and the length of $W_{18}O_{49}$ nanocrystals (**Table 1**). Moreover, the synthesis can be easily done using a big autoclave to prepare $W_{18}O_{49}$ nanowires at large scale (Figure S2, Supporting Information), up to more than one gram in our test, making our finding together with the dimension control very relevant for applications.

In the X-ray diffraction (XRD) pattern in Figure 1f, all the peaks are assigned to the monoclinic $W_{18}O_{49}$ phase (JCPDS no. 005–0392). The growth of tungsten oxide nanowires appears to be along the [010] direction from the narrow and intense (010) peak, which is in good conformity with our high resolution TEM (HRTEM) analysis and earlier literature.[22] X-ray photoelectron spectroscopy (XPS) confirms the presence of W, O, C, and N elements in the M-$W_{18}O_{49}$ nanowires sample with a W/O ratio of 1/2.77, which indicates the existence of oxygen vacancies within the $W_{18}O_{49}$ nanowires (Figure 1g). [23]

2.2. Growth Mechanism of $W_{18}O_{49}$ Nanowires

In order to better understand the growth process, we studied the effect of surfactant concentration. It is well known that the precursor and surfactant concentrations have significant effects on both the size and morphology of nanocrystals. Consequently, we synthesized $W_{18}O_{49}$ nanocrystals from the wet H_2WO_4 precursor (isopropanol-exchanged) with different oleylamine quantities added under constant reaction conditions. The prepared $W_{18}O_{49}$ nanowires with different oleylamine concentrations have all similar dimensions (Figure S3, Supporting Information) which is different to the growth of $W_{18}O_{49}$ nanowires from $W(CO)_6$ and WCl_6 precursors.[8,10] Furthermore, the quantity of white undecomposed H_2WO_4 precursors gradually decreases with increasing the oleylamine volume, which can be observed from the centrifuged white deposition. In the present decomposition of H_2WO_4, oxygen and oxygen containing chemicals have also a strong influence on the formation of $W_{18}O_{49}$ nanowires. For the addition of 2 mL oleic acid, $W_{18}O_{49}$ nanowires with a larger diameter of ≈4–5 nm are obtained (Figure S4b, Supporting Information), while an oleic acid quantity higher than that of oleylamine causes the formation of aggregated WO_3 nanorods with a large diameter of 30 nm (Figure S4c, Supporting Information). This indicates that the decomposition of the wet H_2WO_4 precursor in oleylamine is a reducing process.[24]

In order to deepen our understanding of the growth mechanism of $W_{18}O_{49}$ nanowires, we performed Fourier transform infrared spectroscopy (FTIR) measurements of precursors and studied the nanowire formation process by TEM. In **Figure 2**a, the distinct peaks centered at 1506 and 1607 cm^{-1} are related to $-NH_3^+$ and confirm the formation of oleylamine tungstate salt in the oleylamine-H_2WO_4 sonicated complexes.[25] The H_2WO_4 precursor in isopropanol is cloudy, but the H_2WO_4 precursor in oleylamine shows a clear dispersion because oleylamine can react with H_2WO_4 to form organic ammonium tungstate.

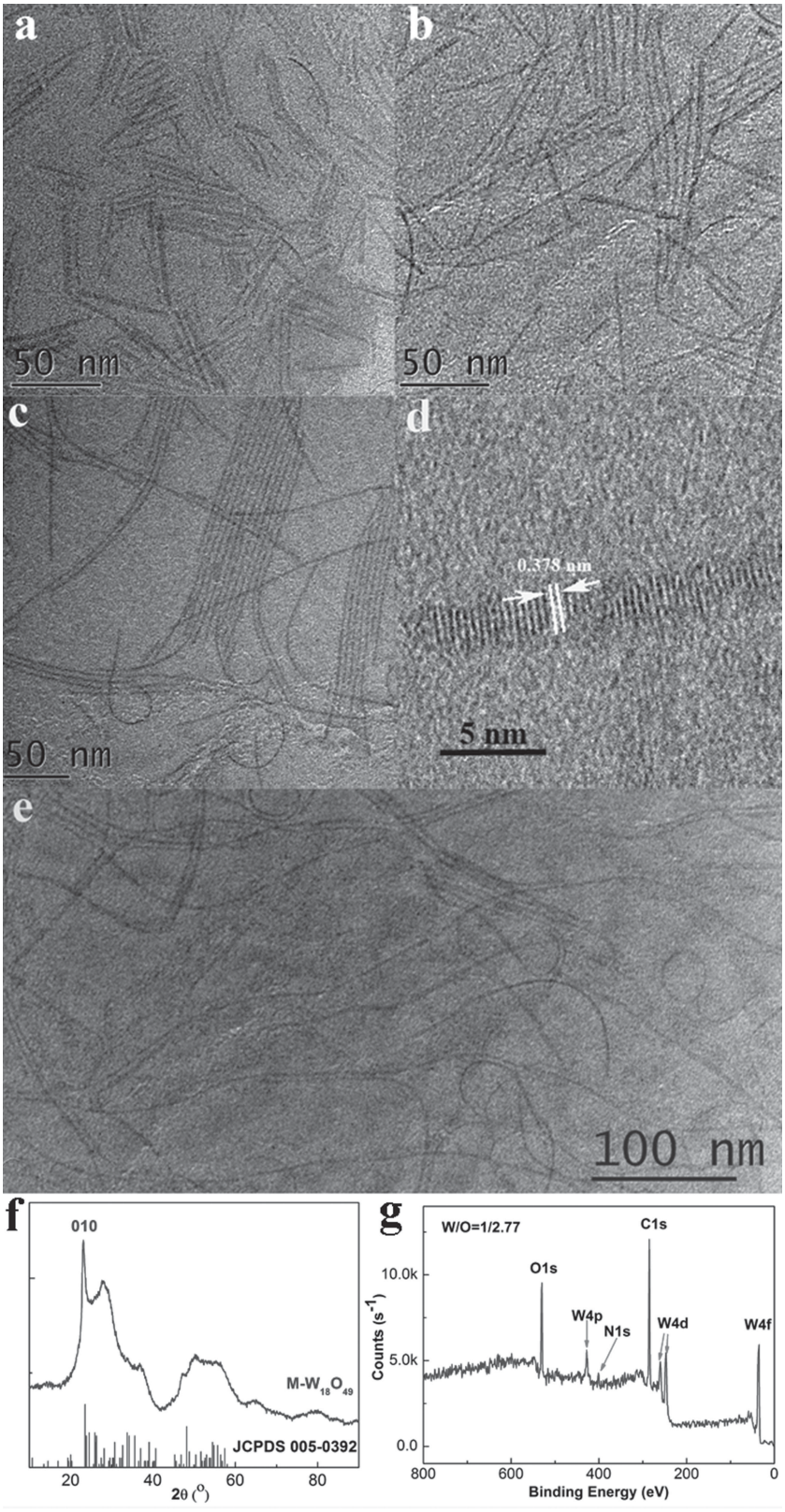

Figure 1. TEM images of the $W_{18}O_{49}$ nanocrystals with a) methanol, b) ethanol, c,d) isopropanol, and e) benzyl alcohol. Figures 1d, 1f, and 1g are the HRTEM image, XRD pattern, and XPS spectrum of Figure 1c.

The TEM image of the dispersed oleylamine-H_2WO_4 composite shows a layered sheet structure with a size of several micrometers (Figure 2b). After the solvothermal reaction for 1 h, the H_2WO_4 sheets decompose into smaller sheets, and several nanorods with a diameter of 40 nm are observed in the TEM image (Figure 2c). After 3 h, the H_2WO_4 sheets become smaller to a size of 50 nm, while the undecomposed H_2WO_4 sheets are surrounded by short $W_{18}O_{49}$ nanowires with a length of about 20–60 nm (Figure 2d). This suggests that nucleation and growth of $W_{18}O_{49}$ nanowires result from the decomposition of H_2WO_4 precursor sheets. After solvothermal reaction for 6 h, a higher quantity of $W_{18}O_{49}$ nanowires with a length of 150 nm can be observed together with little undecomposed H_2WO_4 precursor. A 12 h reaction leads to homogenous $W_{18}O_{49}$ nanowires with a length of about 150 nm (Figure 2e,f), and all the H_2WO_4 precursors were decomposed as indicated by the lack of white deposit after centrifugation of the samples in toluene. After keeping the reaction for 24 h, the diameter of the $W_{18}O_{49}$ nanowires increases to 3–5 nm, resulting from inter-nanowire coupling into bigger nanowires (Figure S5, Supporting Information).[26]

The growth process was also monitored by UV-vis absorption spectra. As shown in Figure 2h, the sample reacted for 1 h shows an absorption onset at 320 nm, which suggests that no $W_{18}O_{49}$ nanocrystals are formed. After 3 h of reaction, the absorption band edge of the synthesized products is at 410 nm, which is related to the main band-to-band absorption of $W_{18}O_{49}$ nanocrystals.[25] With the increase of reaction time, absorption in the visible and near infrared region caused by oxygen vacancies becomes stronger,[27,28] and the dispersion of $W_{18}O_{49}$ nanowires after 12 h of solvothermal reaction shows a deep blue color (Figure 2g).

The growth speed of $W_{18}O_{49}$ nanowires with different wet H_2WO_4 precursors is also different. The wet H_2WO_4 precursor with exchange of water by benzyl alcohol decomposes much faster than that with exchange of water by isopropanol. When using benzyl alcohol, after 1 h more $W_{18}O_{49}$ nanowires are produced and the sizes of the remaining H_2WO_4 precursors are much smaller than those using isopropanol (compare Figure 2c,i).

As reported in earlier works, H_2WO_4 possesses a layered structure, which is made of distorted $WO_5(H_2O)$ octahedrons in a corner

Table 1. Summary of the different samples depending on the alcohol used.

Alcohol used with H_2WO_4	Diameter (nm)	Length (nm)	Sample name	TEM
Methanol	≈2.3–3.3	50	S-$W_{18}O_{49}$ NR	Figure 1a
Ethanol	≈2–2.3	100		Figure 1b
Isopropanol	≈1.7–2	≈120–150	M-$W_{18}O_{49}$ NW	Figure 1c
Benzyl alcohol	1.4	400	L-$W_{18}O_{49}$ NW	Figure 1e

sharing mode.[29,30] Sugahara et al. reported that *n*-alkylamines can be intercalated into the layers of crystalline $H_2W_2O_7 \cdot xH_2O$ and exfoliate crystalline $H_2W_2O_7 \cdot xH_2O$ into single layer sheets after long time stirring for 48 h.[31,32] However, the H_2WO_4 used in our synthesis is amorphous (Figure S6, Supporting Information), and during the washing process by all kinds of alcohols, the water between the different H_2WO_4 layers is supposed to be replaced by alcohol. The replacement of water by alcohol can indeed break the van der Waals forces between the H_2WO_4 layers, which allows the H_2WO_4 precursors to be decomposed more easily at a relatively low temperature of 220 °C. During the decomposition process, the layered H_2WO_4 structure is decomposed into smaller layers of different sizes. Then the two octahedral W-O layers combine with each other to form monoclinic $W_{18}O_{49}$ nuclei without distortion owing to the alcohol removal at high temperatures. The monoclinic $W_{18}O_{49}$ nuclei follow a growth along the [010] direction resulting in nanorod or nanowire formation with the protection of oleylamine on the edges. With the increase of the molecular size of the alcohol, the H_2WO_4 precursor decomposes faster into smaller layered H_2WO_4 units, and $W_{18}O_{49}$ nanowires with smaller diameter and longer length could be obtained.

In order to better understand the effect of the intercalated alcohols, we tried to exchange the water of deposited H_2WO_4 by acetone twice at first, and then we mixed the acetone-exchanged H_2WO_4 precursors with oleylamine and isopropanol. However, only $W_{18}O_{49}$ nanowires with a diameter of 3–7 nm in addition to several large nanorods with a diameter larger than 10 nm are produced (Figure S7, Supporting Information). This suggests that the direct replacement of interlayer water in H_2WO_4

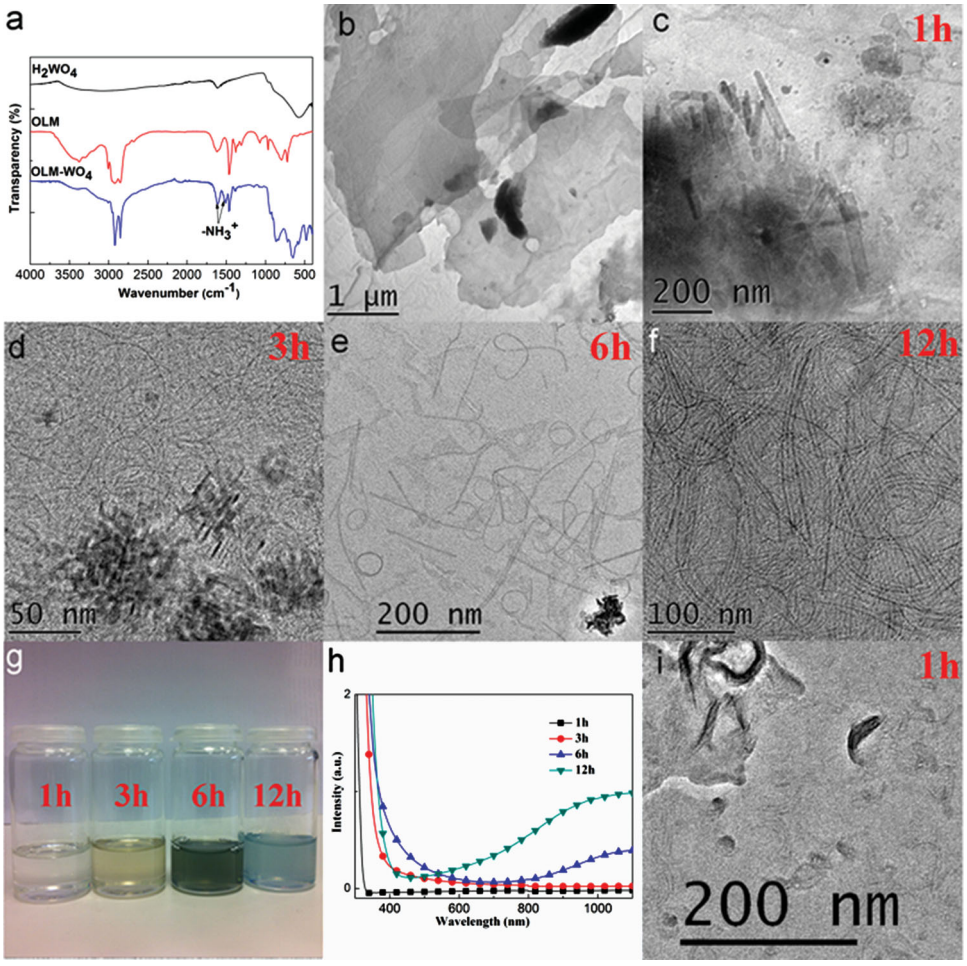

Figure 2. a) FTIR spectra of H_2WO_4, oleylamine, and the oleylamine-H_2WO_4 composite. b) TEM image of the oleylamine-H_2WO_4 composite. c,d,e,f) TEM images of 110 mg isopropanol-intercalated H_2WO_4 in 12 mL oleylamine after solvothermal reaction for 1, 3, 6, and 12 h. g) Photograph of the $W_{18}O_{49}$ dispersion at different reaction times. h) UV-vis absorption spectra of synthesized $W_{18}O_{49}$ at different reaction times. i) TEM image of 110 mg benzyl alcohol-intercalated H_2WO_4 in 12 mL oleylamine after solvothermal reaction for 1 h.

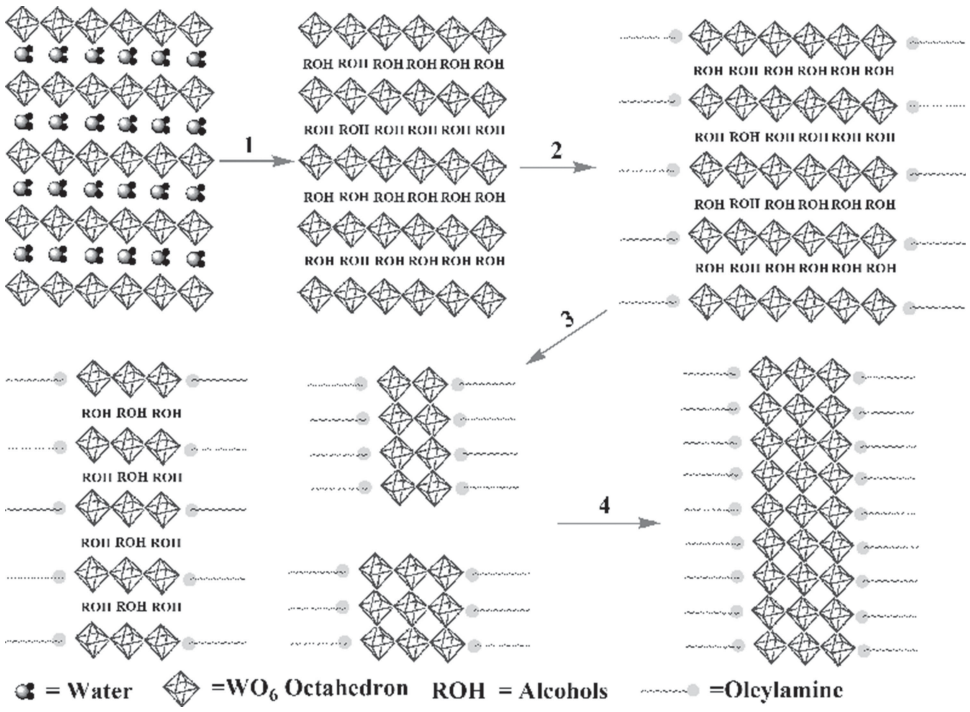

Figure 3. Schematic illustration of the growth mechanism of $W_{18}O_{49}$ nanowires. 1) Replacement of water by alcohol; 2) mixing with oleylamine; 3) decomposition of intercalated tungstic acid and nucleation of $W_{18}O_{49}$; 4) growth of $W_{18}O_{49}$ nanowires.

by alcohol is an indispensible step for the synthesis of ultrathin $W_{18}O_{49}$ nanowires in our reaction system.

From all these experiments, a possible growth mechanism of $W_{18}O_{49}$ nanowires can be summarized (**Figure 3**) as follows: 1) exchange of water between the H_2WO_4 layers by alcohol or the intercalation of alcohol between the H_2WO_4 layers; 2) formation of tungstate oleylamine salt; 3) decomposition of H_2WO_4 precursors and nucleation of $W_{18}O_{49}$ nanowires; and 4) growth of $W_{18}O_{49}$ nanowires.

2.3. Photocatalytic Application of $W_{18}O_{49}$ Nanowires Under Solar Light Irradiation

As the prepared ultrathin $W_{18}O_{49}$ nanowires are highly soluble, exhibit a large surface area combined with direct charge transfer paths inside the long wires, and show a high concentration of oxygen vacancies, these nanomaterials are promising for photocatalytic applications. Although the morphology effect of hierarchical WO_3 spheres on the photocatalytic activity was studied in several works,[33–36] the influence of the aspect ratio of one-dimensional WO_3 nanowires on their photocatalytic activity has never been reported. We thus investigate the photocatalytic activity of as prepared 1 mg mL^{-1} solutions of $W_{18}O_{49}$ nanowires of different aspect ratio via the degradation of 0.25 mg mL^{-1} rhodamine B (RhB) under solar light irradiation.

Taking into account the different aspect ratio of the obtained $W_{18}O_{49}$ nanowires, the total surface of the $W_{18}O_{49}$ nanowires in solution is 32% and 50% larger for the longest L-$W_{18}O_{49}$ NW compared to the medium M-$W_{18}O_{49}$ and small S-$W_{18}O_{49}$ ones, respectively. Beside the difference in surface area, it is known that the adsorption of dye, light absorption, and the charge recombination mechanisms play very important roles in the photocatalytic activity and the removal of pollutants.[39] **Figure 4**a shows UV-vis absorption spectra of RhB after mixing with different $W_{18}O_{49}$ nanomaterials in the dark for 1 h. The adsorbed RhB quantities are 32%, 38%, and 52% for S-$W_{18}O_{49}$ NR, M-$W_{18}O_{49}$ NW, and L-$W_{18}O_{49}$ NW, respectively (Figure 4b). Thus, L-$W_{18}O_{49}$ nanowires show higher adsorption capability than S-$W_{18}O_{49}$ and M-$W_{18}O_{49}$ nanowires, which is in accordance with their larger surface area.

Figure 5a shows the UV-vis absorption of RhB during the photocatalytic degradation process caused by the L-$W_{18}O_{49}$ NW. After 40 min, most of RhB is degradated and the maximum absorption peak of RhB shifted gradually from 554 nm to 499 nm, which is caused by *N*-deethylation of RhB during irradiation.[37,38] Without any photocatalyst, the absorption spectrum of RhB shows no apparent change under the simulated solar light irradiation for 2.5 h, as shown in Figure 5b. Furthermore, Figure 5b compares the photocatalytic degradation of RhB as a function of the aspect ratio of the $W_{18}O_{49}$ nanowires. It can be seen that the L-$W_{18}O_{49}$ NW reduce nearly 80% of RhB during only 40 min irradiation, while the S-$W_{18}O_{49}$ NR and M-$W_{18}O_{49}$ NW show a lower performance of only 47% and 52% of RhB degradation, respectively. Importantly, these values are obtained on a much longer time scale of 2.5 h. The photocatalytic reaction can be simply described by $dC/dt = kC$, where C is the concentration of RhB and k denotes the overall degradation rate constant. The k (min^{-1}) values for S-$W_{18}O_{49}$, M-$W_{18}O_{49}$ and L-$W_{18}O_{49}$ are 0.01293 min^{-1}, 0.01483 min^{-1}, and 0.09476 min^{-1}, respectively (Figure 5c). Thus, the photocatalytic kinetic constant of the L-$W_{18}O_{49}$ NW is 6.4 and therefore

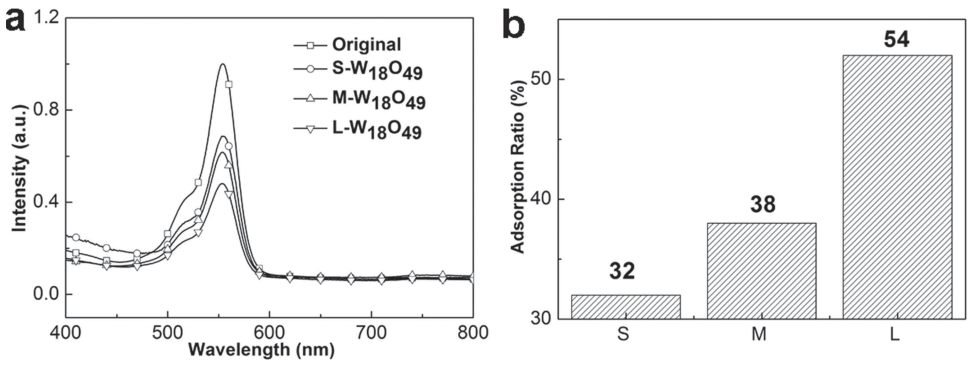

Figure 4. a) UV-vis absorption spectra of the original RhB solution and the RhB solution mixed with $W_{18}O_{49}$ nanocrystals (after 1 h). b) Related adsorption ratios of S-, M-, and L-$W_{18}O_{49}$ nanocrystals.

7.3 times higher than that of M-$W_{18}O_{49}$ and S-$W_{18}O_{49}$, indicating a significantly higher photocatalytic activity of $W_{18}O_{49}$ NW with increasing the aspect ratio. L-$W_{18}O_{49}$ NW also shows high photocatalytic activity after 3 recycling experiments, which takes on a small range drop compared with that in the first cycling experiment (Figure 5d).

The effect of light absorption is also studied for the three aspect ratios, taking into account the evolution of absorption after multiple photocatalytic cycles. In **Figure 6**a, with a similar main band gap absorption at around 410 nm, L-$W_{18}O_{49}$ NW shows stronger absorption in the visible and near infrared region compared to the medium and short ones, mainly caused

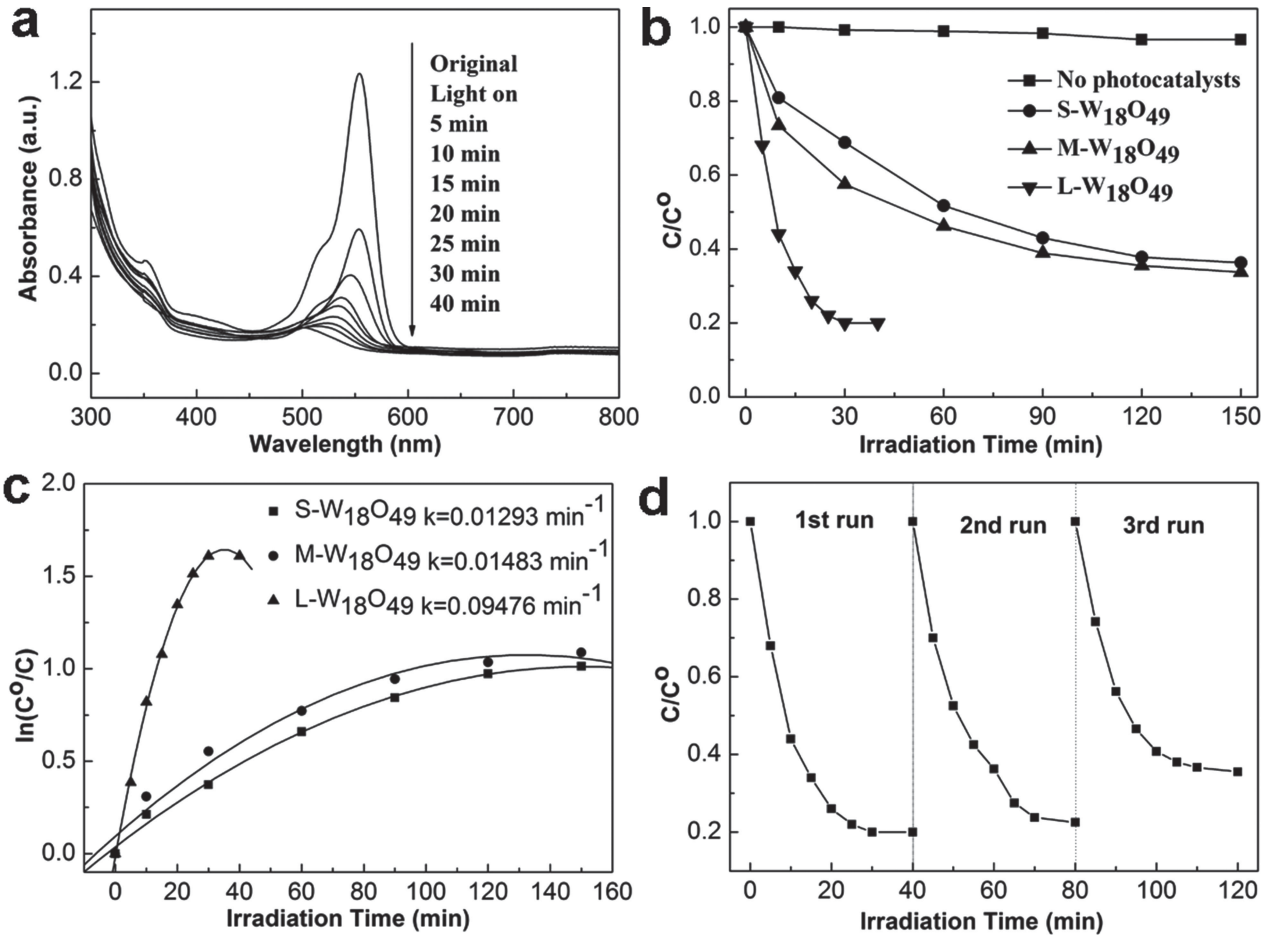

Figure 5. a) UV-vis spectroscopic changes of the RhB aqueous solution in the presence of L-$W_{18}O_{49}$ NW. b) Photocatalytic degradation of RhB by S-$W_{18}O_{49}$ NR, M-$W_{18}O_{49}$ NW, and L-$W_{18}O_{49}$ NW. c) Kinetic plots for S-$W_{18}O_{49}$ NR, M-$W_{18}O_{49}$ NW, and L-$W_{18}O_{49}$ NW. d) Recyclability of the photocatalytic decomposition of RhB by L-$W_{18}O_{49}$ NW.

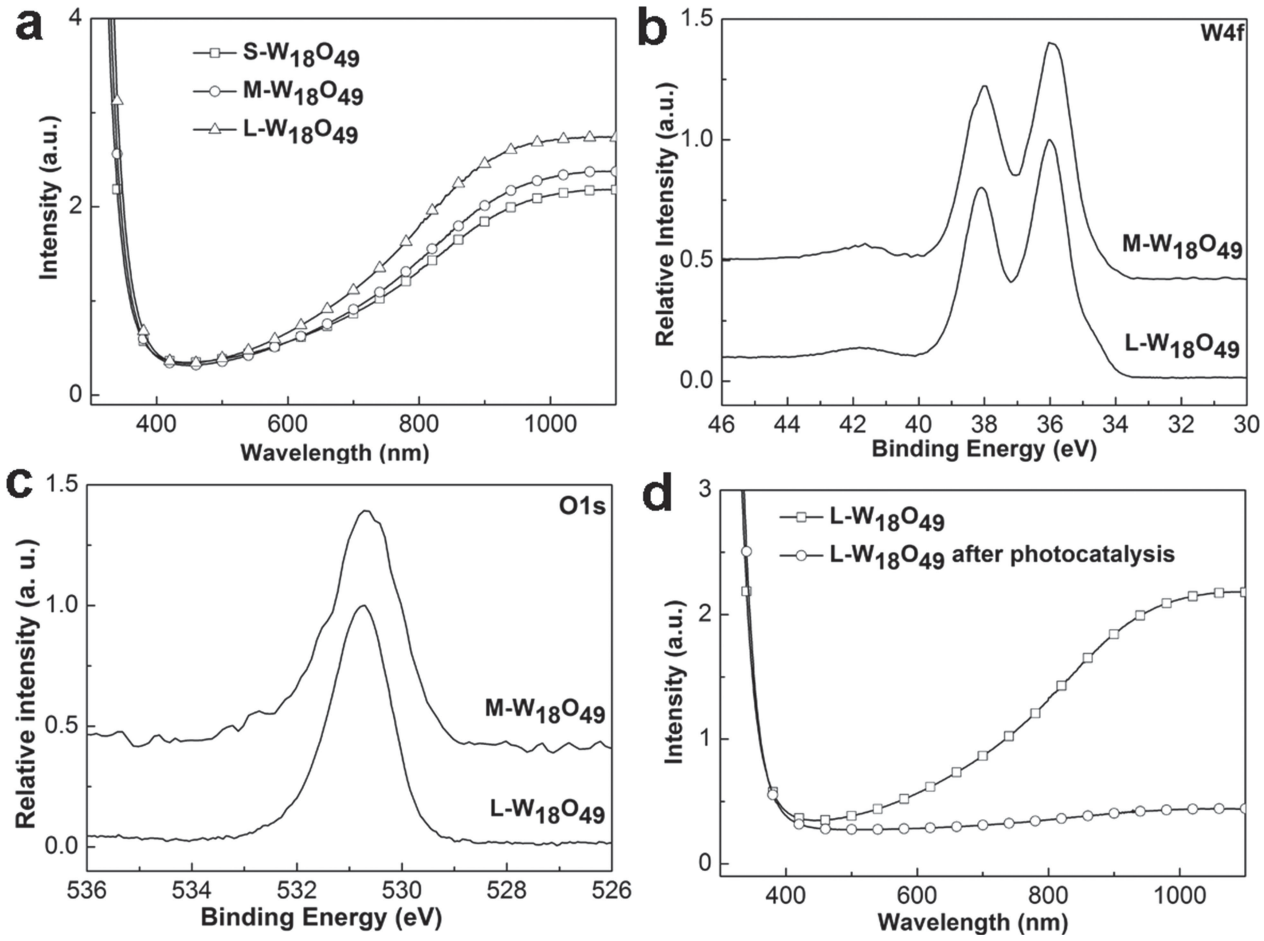

Figure 6. a) UV-vis absorption spectra of S-$W_{18}O_{49}$ NR, M-$W_{18}O_{49}$ NW, and L-$W_{18}O_{49}$ NW. b) High-resolution W4f core-level spectra. c) High-resolution O1s core-level spectra. d) UV-vis absorption of L-$W_{18}O_{49}$ NW before and after 2 cycles of photocatalytic reaction.

by oxygen vacancies. This is explained by the lower oxygen content and higher W^{5+} defects in L-$W_{18}O_{49}$ NW, which was confirmed by the XPS W4f and O1s spectra (Figure 6b,c). The O/W ratio for L-$W_{18}O_{49}$ NW is 2.7, which is lower than 2.77 for the M-$W_{18}O_{49}$ NW. It could be concluded at this stage that the W^{5+} defects and the oxygen vacancies play important roles on both the visible light absorption and the photocatalytic activity under solar light irradiation. Another observation gives additional insights: after the second cycle of photocatalytic reaction, the color of L-$W_{18}O_{49}$ nanomaterials changes from blue to white, and shows much weaker absorption in the visible light area (Figure 6d) while the XRD patterns stay unchanged (Figure S8, Supporting Information). The change in color from blue to white indicates that after these two cycles, less oxygen defects are present. However, these white L-$W_{18}O_{49}$ NW after two cycles could still degradate 64% of RhB (third run, Figure 5d), which is more than for blue S-$W_{18}O_{49}$ and M-$W_{18}O_{49}$ NW after the first cycle. This suggests that not only the amount of defect states plays a role in the photodegradation of RhB, but also the aspect ratio significantly affects the photocatalytic activity of $W_{18}O_{49}$ nanocrystals. With increasing the aspect ratio, L-$W_{18}O_{49}$ NW can provide a direct charge transfer path and effectively prevent the charge recombination.[40,41]

3. Conclusions

A novel solvothermal decomposition method using low-cost, non-toxic starting materials in a one-step reaction has been developed, which allows synthesizing high-quality, ultrathin $W_{18}O_{49}$ nanowires on a gram-scale with different aspect ratios. The length of the one-dimensional $W_{18}O_{49}$ nanocrystals was adjusted to 50–400 nm, while the diameter could be controlled to 3.3–1.4 nm by simply changing the alcohol during the synthesis. The monoclinic crystal structure and a high concentration of oxygen defects of the ultrathin $W_{18}O_{49}$ nanowires was confirmed by XRD and XPS analysis. By studying the photocatalytic degradation of RhB by the nanowires, we could demonstrate that significantly enhanced photocatalytic activity, improved degradation kinetics, and remarkable stability exist for the longest $W_{18}O_{49}$ nanowires. This was assigned to the synergistic effects of the high adsorption of RhB, the presence of more oxygen defects, and the higher aspect ratio. This new top-down synthetic method will open a new route for the growth of ultrathin nanowires from the decomposition of bulk precursors, and may be extended to the synthesis of two-dimensional graphene-like inorganic nanosheets.

4. Experimental Section

Materials: Concentrated nitric acid (70%), oleylamine (70%), rhodamine B (99%), sodium tungstate dihydrate ($Na_2WO_4.2H_2O$, 99%), and oleic acid (90%) were purchased from Aldrich. All solvents were purchased from Merck Ltd. Deionized (DI) water was produced in our lab.

Synthesis of Ultrathin Tungsten Oxide Nanowires: Ultrathin tungsten oxide nanowires were synthesized by a solvothermal method. Typically, 110 mg of Na_2WO_4 were dissolved in 3 ml DI water, and then 3 ml of 7% HNO_3 aqueous solution was added into the Na_2WO_4 solution. The light yellow deposition of H_2WO_4 was formed immediately and was centrifuged to get a solid which was washed with isopropanol (or methanol, ethanol, benzyl alcohol, or acetone) for 2 times. Then ≈4–16 mL of oleylamine was added to the H_2WO_4 deposition. The mixture was sonicated at room temperature for 20 min to get clear solutions. The mixed solution was then transferred into a 45 mL autoclave, and purged with argon for 15 min. The autoclave was then put into an electronic oven under 220 °C for 12 h. The $W_{18}O_{49}$ product was then deposited by adding 40 mL of ethanol and washed twice with absolute ethanol. The prepared $W_{18}O_{49}$ products were redispersed in toluene for further TEM observation and other characterizations. For large-scale synthesis, 1.5 g of Na_2WO_4 in 10 ml DI water and 10 ml of 7% HNO_3 were mixed to get the H_2WO_4 deposition. Then the alcohol washing process was the same as the aforementioned synthesis process. The produced alcohol-intercalated H_2WO_4 and 70 ml of oleylamine were mixed and sonicated for 20 min. At last the H_2WO_4 and oleylamine mixture were put in a 125 ml autoclave for the solvothermal process at 220 °C for 12 h.

Characterization: TEM and HRTEM images were obtained using a JEOL 3010-H microscope (TEM) operating at 300 kV. The samples for the analysis were prepared by dropping dilute toluene solutions of $W_{18}O_{49}$ nanowires onto 400-mesh carbon-coated copper grids and leaving the solvent to dry. Powder diffraction measurements were realized using an INEL diffractometer equipped with a 120° curved position sensitive detector (CPS-120), operation power: 45 kV and 20 mA. FTIR spectra were recorded on a Perkin Elmer GX FT-IR system using the compressed KBr disc technique. UV-vis absorption spectra were recorded by using a Cary 5000 UV-Vis-NIR spectrophotometer. XPS measurements were carried out by using a Kratos Axis Ultra Spectrometer with a monochromic Al Ka source at 1486.7 eV, with a voltage of 15 kV and an emission current of 10 mA.

Photocatalytic Experiments: The degradation of rhodamine B under simulated solar light irradiation (140 W, Oriel Sol1A AM 1.5 pure simulated solar light) was observed based on the absorption spectroscopic technique. Typically, aqueous solutions of the RhB dyes (0.5 mL of 0.005 g L^{-1} solution) and the $W_{18}O_{49}$ photocatalysts (50 mg dispersed in 49.5 mL of DI water) were placed in a glass beaker of 100 mL. After stirring for 1 h in the dark to reach the adsorption equilibrium, the photoreaction vessel was exposed to solar-light irradiation. Before mixing with RhB, the $W_{18}O_{49}$ nanowires were washed with hexane and ethanol for 3 times, and were sonicated to get good dispersions in DI water. The photocatalytic reaction was started by turning on the lamp, while all other lights were insulated during the photocatalysis. After given time intervals, 5 mL of the photo-reacted solution were analyzed by recording variations of the absorption band maximum in the UV-vis spectra of RhB.

Supporting Information

Supporting Information is available from the Wiley Online Library or from the author.

Acknowledgements

This work was supported by the SFUMATO – FUI Project AAP12. The authors thank Serge Nitsche, Damien Chaudanson, and Vasile Heresanu from CINaM for their assistance in the use of the TEM and XRD facilities.

Received: April 19, 2014
Published online: July 29, 2014

[1] L. Cademartiri, G. A. Ozin, *Adv. Mater.* **2009**, *21*, 1013–1020.
[2] S. Hu, X. Wang, *Chem. Soc. Rev.* **2013**, *42*, 5577–5594.
[3] A. Repko, L. Cademartiri, *Can. J. Chem.* **2012**, *90*, 1032–1047.
[4] B. Aurian-Blajeni, M. Halmann, J. Manassen, *Sol. Energy* **1980**, *25*, 165–170.
[5] R. Abe, H. Takami, N. Murakami, B. Ohtani, *J. Am. Chem. Soc.* **2008**, *130*, 7780–7781.
[6] H. Zheng, J. Z. Ou, M. S. Strano, R. B. Kaner, A. Mitchell, K. Kalantar-zadeh, *Adv. Funct. Mater.* **2011**, *21*, 2175–2196.
[7] A. L. Stroyuk, A. I. Kryukov, S. Y. Kuchmii, V. D. Pokhodenko, *Theor. Exp. Chem.* **2005**, *41*, 207–228.
[8] H. G. Choi, Y. H. Jung, D. K. Kim, *J. Am. Ceram. Soc.* **2005**, *88*, 1684–1686.
[9] G. Xi, S. Ouyang, P. Li, J. Ye, Q. Ma, N. Su, H. Bai, C. Wang, *Angew. Chem. Int. Ed.* **2012**, *51*, 2395–2399.
[10] J. Polleux, A. Gurlo, N. Barsan, U. Weimar, M. Antonietti, M. Niederberger, *Angew. Chem. Int. Ed.* **2005**, *45*, 261–265.
[11] B. Moshofsky, T. Mokari, *Chem. Mater.* **2013**, *25*, 1384–1391.
[12] X. W. Lou, H. C. Zhen, *Inorg. Chem.* **2003**, *42*, 6169–6171.
[13] J. Rajeswari, P. S. Kishore, B. Viswanathan, T. K. Varadarajan, *Nanoscale Res. Lett.* **2007**, *2*, 496–503.
[14] J. Wang, E. Khoo, P. S. Lee, J. Ma, *J. Phys. Chem. C* **2008**, *112*, 14306–14312.
[15] S. Bai, K. Zhang, R. Luo, D. Li, A. Chen, C. C. Liu, *J. Mater. Chem.* **2012**, *22*, 12643–12650.
[16] X. L. Li, J. F. Liu, Y. D. Li, *Inorg. Chem.* **2003**, *42*, 921–924.
[17] Z. Gu, H. Li, T. Zhai, W. Yang, Y. Xia, Y. Ma, J. Yao, *J. Solid State Chem.* **2007**, *180*, 98–105.
[18] X. Q. Gao, F. Xiao, C. Yang, J. D. Wang, X. T. Su, *J. Mater. Chem. A* **2013**, *1*, 5831–5834.
[19] J. Polleux, N. Pinna, M. Antonietti, M. Niederberger, *J. Am. Chem. Soc.* **2005**, *12*, 15595–15601.
[20] P. Kalluru, R. Vankayala, C. Chiang, K. C. Hwang, *Angew. Chem. Int. Ed.* **2013**, *52*, 12332–12336.
[21] C. Guo, S. Yin, M. Yan, M. Kobayashi, M. Kakihana, T. Sato, *Inorg. Chem.* **2012**, *51*, 4763–4771.
[22] Z. Chen, Q. Wang, H. Wang, L. Zhang, G. Song, L. Song, J. Hu, H. Wang, J. Liu, M. Zhu, D. Zhao, *Adv. Mater.* **2013**, *25*, 2095–2100.
[23] T. Nutz, M. Haase, *J. Phys. Chem. B* **2000**, *104*, 8430–8437.
[24] N. Soultanidis, W. Zhou, C. J. Kiely, M. S. Wong, *Langmuir* **2012**, *28*, 17771–17777.
[25] B. Ingham, S. V. Chong, J. L. Tallon, *J. Phys. Chem. B* **2005**, *109*, 4936–4940.
[26] M. R. Waller, T. K. Townsend, J. Zhao, E. M. Sabio, R. L. Chamousis, N. D. Browning, F. E. Osterloh, *Chem. Mater.* **2012**, *24*, 698–704.
[27] T. Nutz, M. Haase, *J. Phys. Chem. B* **2000**, *104*, 8430–8437.
[28] K. Manthiram, A. P. Alivisatos, *J. Am. Chem. Soc.* **2012**, *134*, 3995–3998.
[29] L. Liang, J. Zhang, Y. Zhou, J. Xie, X. Zhang, M. Guan, B. Pan, Y. Xie, *Sci. Rep.* **2013**, *3*, 1936.
[30] J. T. Szymanski, A. C. Roberts, *Can. Mineral.* **1984**, *22*, 681–688.
[31] D. Chen, Y. Sugahara, *Chem. Mater.* **2007**, *19*, 1808–1815.
[32] D. Chen, T. Li, L. Yin, X. Hou, X. Yu, Y. Zhang, B. Fan, H. Wang, X. Li, R. Zhang, T. Hou, H. Lu, H. Xu, J. Sun, L. Gao, *Mater. Chem. Phys.* **2011**, *125*, 838–845.
[33] G. Xi, Y. Yan, Q. Ma, J. Li, H. Yang, X. Lu, C. Wang, *Chem. Eur. J.* **2012**, *18*, 13949–13953.
[34] D. Chen, J. Ye, *Adv. Funct. Mater.* **2008**, *18*, 1922–1928.

[35] G. Xi, B. Yue, J. Cao, J. Ye, *Chem. Eur. J.* **2011**, *17*, 5145–5154.
[36] H. Bai, N. Su, W. Li, X. Zhang, Y. Yan, P. Li, S. Ouyang, J. Ye, G. Xi, *J. Mater. Chem. A* **2013**, *1*, 6125–6129.
[37] T. Watanabe, T. Takizawa, K. Honda, *J. Phys. Chem.* **1977**, *81*, 1845–1851.
[38] J. Zhuang, W. Dai, Q. Tian, Z. Li, L. Xie, J. Wang, P. Liu, *Langmuir* **2010**, *26*, 9686–9694.
[39] J. Liu, H. Bai, Y. Wang, Z. Liu, X. Zhang, D. D. Sun, *Adv. Funct. Mater.* **2010**, *10*, 4175–4181.
[40] W. U. Huynh, J. J. Dittmer, A. P. Alivisatos, *Science* **2002**, *295*, 2425–2427.
[41] N. Wu, J. Wang, D. N. Tafen, H. Wang, J. G. Zheng, J. P. Lewis, X. Liu, S. S. Leonard, A. Manivannan, *J. Am. Chem. Soc.* **2010**, *132*, 6679–6685.